MAE 263F Final Report - Parachutes in Flight

Lovleen Kaur and Abinav Ramachandran Kamalakannan

I. INTRODUCTION

Parachutes are deployed and used in a varying applications ranging from aerospace, human descent and cargo delivery. Understanding the complex fluid-structure interactions during the deployment of a parachute is essential in developing robust and safe parachutes. By creating a numerical solver to study this behavior under various conditions, we hope to gain valuable insight on which factors affect the functioning of a parachute the most.

The numerical simulation frameworks used in this project is based on discrete elastic rods (DER) with hydrodynamic forces and additional section of work using Shells with hydrodynamic forces. Using numerical methods like Newton-Rhapson, we aim to simulate the forces and motion of the canopy, cords and the load. For the sake of simplicity, we avoid simulating the complex fluid flow around the parachute and have a simplified model to approximate the aerodynamic drag on the canopy.

The primary objectives of this study is to examine the steady state canopy profile under steady descent, and to determine the terminal velocities achieved across a range of operating parameters and simulation methods. We compared the terminal velocity and the canopy profile using DER simulation under three different loads that are varied by one order of magnitude for each increase. Also also performed a simulation with Shells with one of same load cases and compared the performance of the simulation and possible courses of error. By studying these metrics of the parachute with different methods, we hope to provide insights on parachute performances under different design choices and environmental conditions.

Extensive work have been previously done in simulating the behavior of deploying parachutes in supersonic regimes [2] and subsonic regimes [5]. Our paper aims to gain a broad understanding of parameters relevant in understanding performance of a parachute in various flow conditions.

II. METHODOLOGY

The main simulation work for this project is done with Hydrodynamics applied with Discrete Elastic Rods algorithm. We estimate the Reynolds number using a characteristic velocity v_{charac}, a characteristic length L_{charac}, fluid density ρ, and viscosity μ:

$$Re = \frac{\rho\, v_{\text{charac}}\, L_{\text{charac}}}{\mu}.$$

A. High Reynolds Number Hydrodynamics (Quadratic Drag)

For high Reynolds number flows ($Re \gg 1$), inertial forces in the fluid dominate and hydrodynamic drag scales quadratically with velocity. Where ρ denotes the fluid density and C_D is the drag coefficient. Each node represents a segment of undeformed Voronoi length l_k and circular radius r_0. The projected area associated with node k is

$$A_k = 2r_0\, l_k.$$

If the background fluid has uniform velocity $\mathbf{U}_\infty$, drag depends on the relative velocity

$$\mathbf{u}_k^{\text{rel}} = \mathbf{u}_k - \mathbf{U}_\infty,$$

where $\mathbf{u}_k$ is the backward–Euler velocity. If no flow is present, $\mathbf{U}_\infty = 0$.

The high–Re drag force at node k is

$$\mathbf{f}_k^{\text{highRe}} = -\tfrac{1}{2}\rho C_D A_k \|\mathbf{u}_k^{\text{rel}}\|\, \mathbf{u}_k^{\text{rel}}.$$

where k is defined as

$$k_k = \tfrac{1}{2}\rho C_D A_k,$$

so that

$$\mathbf{f}_k^{\text{highRe}} = -k_k\, \|\mathbf{u}_k^{\text{rel}}\|\, \mathbf{u}_k^{\text{rel}}.$$

Jacobian of the High-Reynolds Drag

Let $g(\mathbf{u}) = \|\mathbf{u}\|\mathbf{u}$. So its differential is

$$dg = \left(\|\mathbf{u}\|\mathbf{I} + \frac{\mathbf{u}\mathbf{u}^T}{\|\mathbf{u}\|}\right) d\mathbf{u}.$$

Thus,

$$\frac{\partial g}{\partial \mathbf{u}} = \|\mathbf{u}\|\mathbf{I} + \frac{\mathbf{u}\mathbf{u}^T}{\|\mathbf{u}\|}.$$

Applied to $\mathbf{u}_k^{\text{rel}}$,

$$\frac{\partial \mathbf{f}_k^{\text{highRe}}}{\partial \mathbf{u}_k^{\text{rel}}} = -k_k \left(\|\mathbf{u}_k^{\text{rel}}\| \mathbf{I} + \frac{\mathbf{u}_k^{\text{rel}} \left(\mathbf{u}_k^{\text{rel}}\right)^T}{\|\mathbf{u}_k^{\text{rel}}\|} \right).$$

Since

$$\frac{\partial \mathbf{u}_k^{\text{rel}}}{\partial \mathbf{x}_k(t_{j+1})} = \frac{1}{\Delta t}\mathbf{I},$$

the Jacobian with respect to DOFs is

$$\frac{\partial \mathbf{f}_k^{\text{highRe}}}{\partial \mathbf{x}_k(t_{j+1})} = -\frac{k_k}{\Delta t} \left(\|\mathbf{u}_k^{\text{rel}}\| \mathbf{I} + \frac{\mathbf{u}_k^{\text{rel}} \left(\mathbf{u}_k^{\text{rel}}\right)^T}{\|\mathbf{u}_k^{\text{rel}}\|} \right).$$

It is zero for all $j \neq k$. The Jacobian is therefore block-diagonal: a 2×2 block for planar rods or 3×3 for 3D rods.

B. High-Reynolds Forces Solver Algorithm

The computation starts with,

$$\mathbf{F}_h = 0_{(n_{\text{dof}})}, \qquad \mathbf{J}_h = 0_{(n_{\text{dof}} \times n_{\text{dof}})},$$

and loops over all nodes k to:

- Compute $\mathbf{u}_k$ and relative velocity $\mathbf{u}_k^{\text{rel}}$.
- Compute projected area $A_k = 2r_0 l_k$.
- Evaluate the high-Re drag force and assemble it into $\mathbf{F}_h$.
- Evaluate the corresponding Jacobian (with regularization if applicable) and assemble it into the (k, k) block of $\mathbf{J}_h$.

C. Discretization of Domain and External Forces:

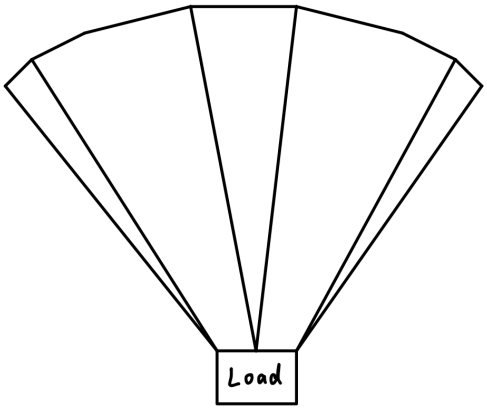

Fig. 1: Discrete Representation of a Parachute and Load

Figure 1 shows the discrete representation of a parachute, each node of the parachute (in black ink) has two main forces acting on it. There is the force of gravity pulling the parachute down and the drag force acting in the opposite direction. The magnitude of the drag force will depend on the shape of the parachute and that is computed by the hydrodynamics force part of the computational scheme. The main assumption is the hydrodynamics logic is the coefficient of drag and that is because the value used is largely an estimation for parachutes after they are deployed fully. This number is highly dependent on the shape of the parachute but for the purposes of this study, the value is held a reasonable constant for the final shape. In reality, the C_D (drag coefficient) varies heavily with the flow conditions, gas composition, and parachute shape. The aim of the project is to study the behaviors of this flexible structure under varied applied loads and material properties. The high fidelity aero-structures coupling analysis or drag profile in transient state of deployment is not the main target of this project. The parachute here is assumed to start flat and expand into its shape. This number is taken from a NASA Glenn Research Center quick information and learning page for basics of parachute dynamics [6].

$$C_D = 1.75$$

The C_D values can be estimated using flight data or from prior higher fidelity simulations. NASA has variety of papers that describe parachute analysis and C_D for different flight envelopes. One such paper provides C_D properties for Mars landing [1]. Another similar resource cover the numerical analyses that details the CFD work necessary to tackle this problem [3]. These sources examine this process much more in depth rather than a simplified constant coefficient like this in case.

D. Implementation of Shells

Additional to the main simulation of the discrete elastic rods, a discrete shell simulation was implemented. The parachute canopy is discretized into triangular shell elements with a spring stiffness for each edge and a bending stiffness along the hinges. Like the DER simulations, each node in the shell experiences the effect of gravity and has a distributed load acting downwards along its edges. Figure 2 and Figure 3 provides the initial position of the shell mesh and the two different loading distributions of 200 N applied to it. For each discrete shell element, the average velocity of all the three nodes is used as the velocity for the particular shell.

The implementation of drag forces on the shell have been modified to include two drag coefficients:

- $C_{D,n} = 1.75$, Normal Drag Coefficient
- $C_{D,t} = 0.5$, Tangential Drag Coefficient

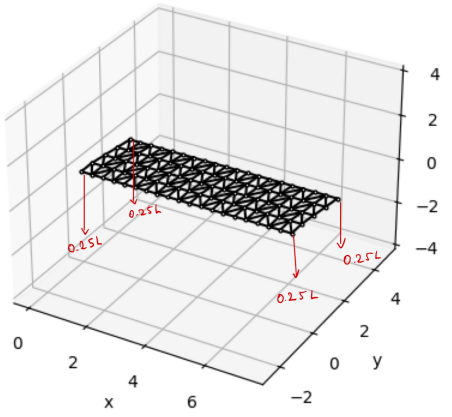

Fig. 2: Shell mesh and loading distribution

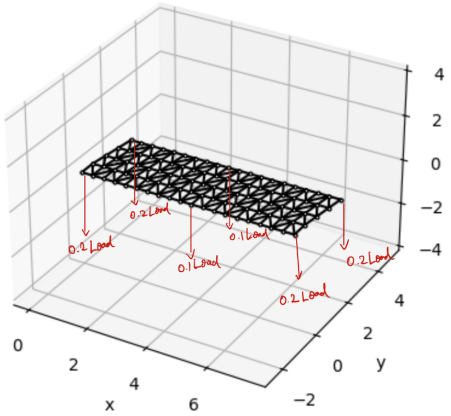

Fig. 3: Shell mesh and loading distribution with a middle load

The normal Drag Coefficient ($C_{D,n}$) is the same as the drag coefficient used in the DER implementation and is used when the relative fluid flow is directed perpendicularly towards the shell. The Tangential Drag Coefficient ($C_{D,t}$) represents the drag caused by the viscous drag force due to the sliding fluid along the shell. The skin friction drag force is significantly smaller when compared to the normal drag force. Additionally, the planform area of each shell is used to measure the normal drag force as there should be no contribution to the normal drag force if the shell is oriented parallel to the relative fluid velocity.

By taking the cross product of two edges for each shell element the normal vector is obtained for every discrete shell element as shown in Figure 4. This normal vector is used to measure the drag forces using the following equation:

$$\mathbf{f}_t^{\text{highRe}} = -\tfrac{1}{2}\rho C_{D,t} A_k \|\mathbf{u}_t^{\text{rel}}\| \, \mathbf{u}_t^{\text{rel}}.$$

$$\mathbf{f}_n^{\text{highRe}} = -\tfrac{1}{2}\rho C_{D,n} A_{proj} \|\mathbf{u}_n^{\text{rel}}\| \, \mathbf{u}_n^{\text{rel}}.$$

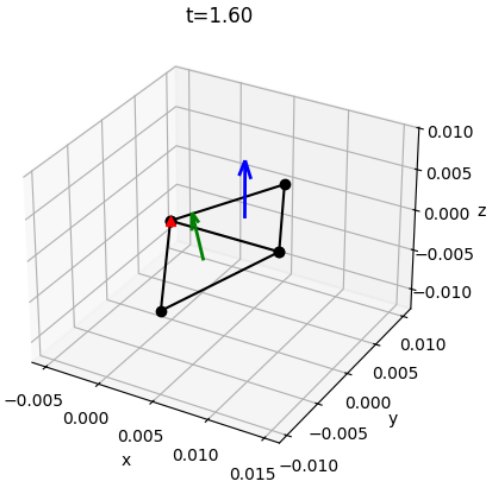

Fig. 4: Normal vector for every shell element

where,

$$A_{proj} = A_k(\hat{\mathbf{n}}_k \cdot \hat{\mathbf{u}}_k^{rel})$$

$$\hat{\mathbf{n}}_k = \hat{e_{k1}} \times \hat{e_{k2}}$$

The implementation of the Jacobian is similar to that of the DER simulation. For the sake of simplicity, it does not factor in the projected area.

$$\mathbf{J}_n = \frac{\partial \mathbf{f}_n^{\text{highRe}}}{\partial \mathbf{u}_{rel}} = -\frac{1}{2}\rho C_{D,n} A_k \left(|\mathbf{u}_n| \mathbf{I} + \frac{\mathbf{u}_n \otimes \mathbf{u}_n}{|\mathbf{u}_n|} \right) \mathbf{P}_n$$

$$\mathbf{J}_t = \frac{\partial \mathbf{f}_t^{\text{highRe}}}{\partial \mathbf{u}_{rel}} = -\frac{1}{2}\rho C_{D,t} A_k \left(|\mathbf{u}_t| \mathbf{I} + \frac{\mathbf{u}_t \otimes \mathbf{u}_t}{|\mathbf{u}_t|} \right) \mathbf{P}_t$$

where,

$$\mathbf{P}_n = \hat{\mathbf{n}} \otimes \hat{\mathbf{n}}$$

$$\mathbf{P}_t = \mathbf{I} - \hat{\mathbf{n}} \otimes \hat{\mathbf{n}}$$

E. Choice of dt:

Time step size depends on the method, the system being analyzed, computational cost, and the speed needed. The selected time step of 0.001 resulted in a solution that converged well and reached a steady state that is a expected of a parachute.

F. Parachute Dimensions and Material:

- High Speed Grade Parachute Kelvar
- Young's Modulus: 55 GPa
- Length: 6m
- Width = 3m
- Thickness = 2mm

III. RESULTS

A. DER: Canopy Final State

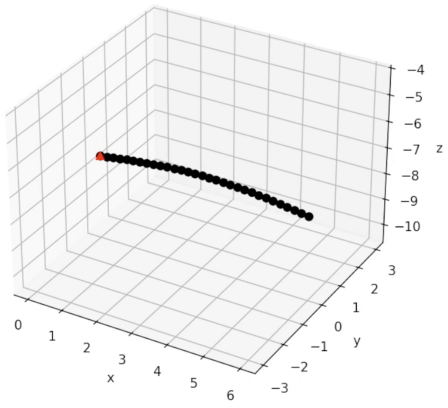

Fig. 5: DER Final State, Load = 20N

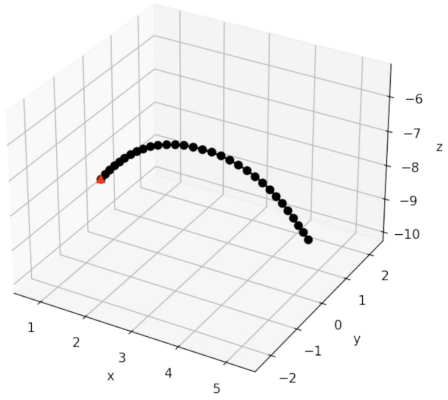

Fig. 6: DER Final State, Load = 200N

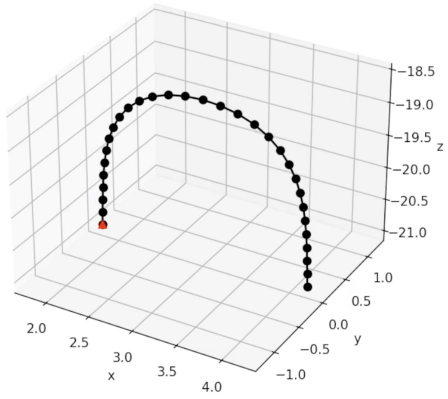

Fig. 7: DER Final State, Load = 2000N

B. DER: Terminal Velocity Profiles

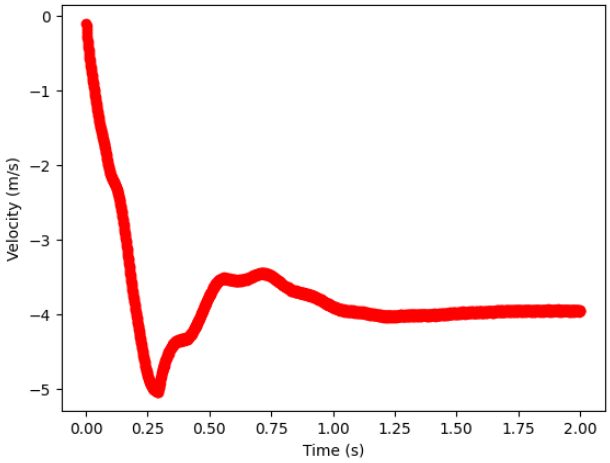

Fig. 8: DER Terminal Velocity, Load = 20N

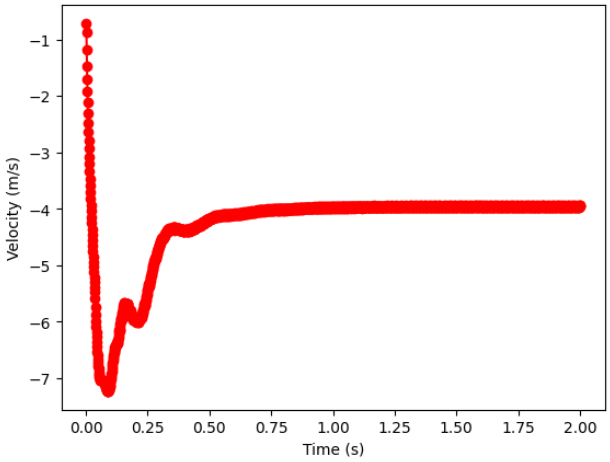

Fig. 9: DER Terminal Velocity, Load = 200N

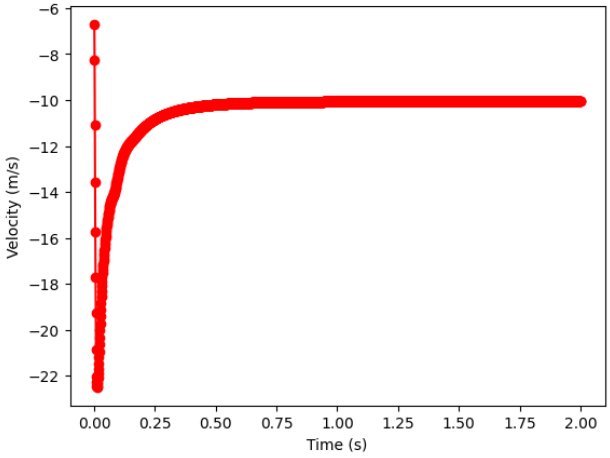

Fig. 10: DER Terminal Velocity, Load = 2000N

C. DER: Maximum Extended Height of Parachute

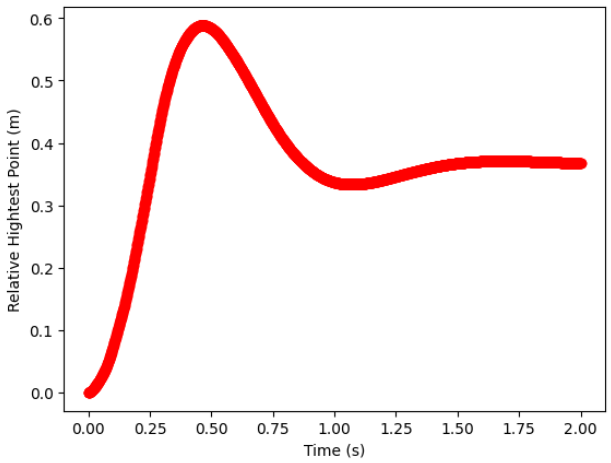

Fig. 11: DER Terminal Velocity, Load = 20N

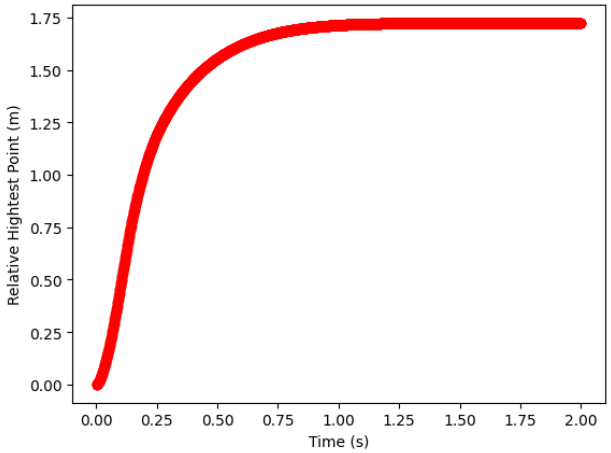

Fig. 12: DER Terminal Velocity, Load = 200N

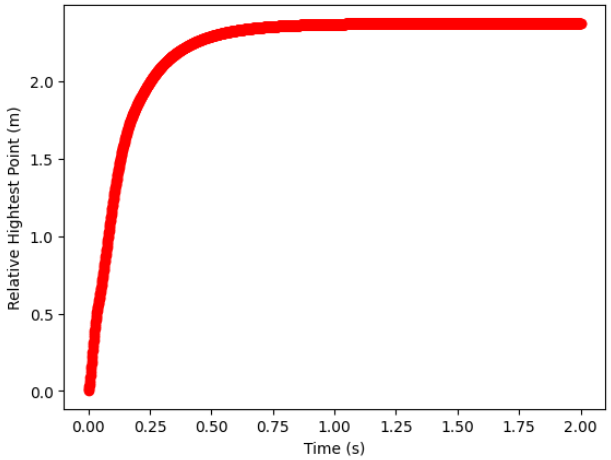

Fig. 13: DER Terminal Velocity, Load = 2000N

D. Shell Simulation (4 Side Loading) Load = 200N

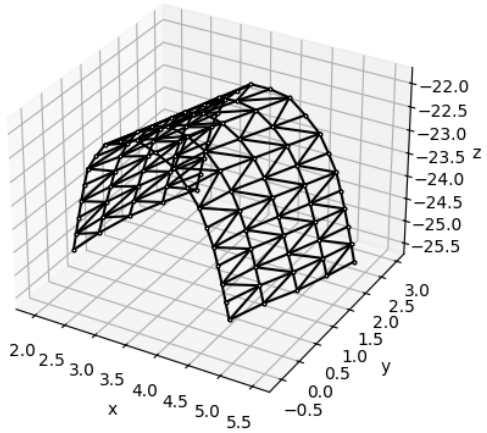

Fig. 14: Shell Simulation at t = 3.00 s, Load = 200N

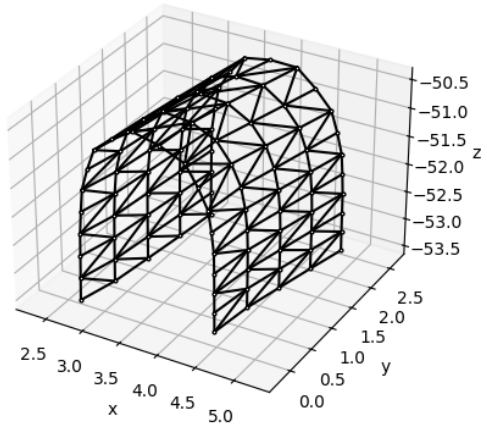

Fig. 15: Shell Simulation at t = 6.00 s, Load = 200N

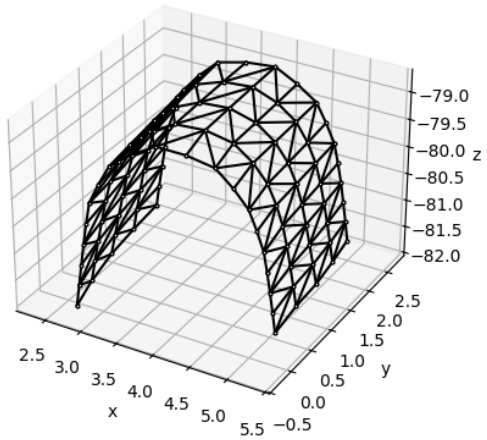

Fig. 16: Shell Simulation at t = 9.00 s, Load = 200N

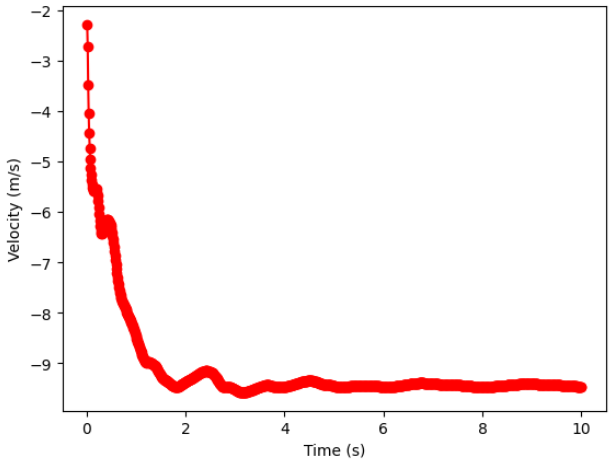

Fig. 17: Shell Simulation Terminal Velocity, Load = 200N

E. Shell Simulation (With Mid Loading) Load = 200N

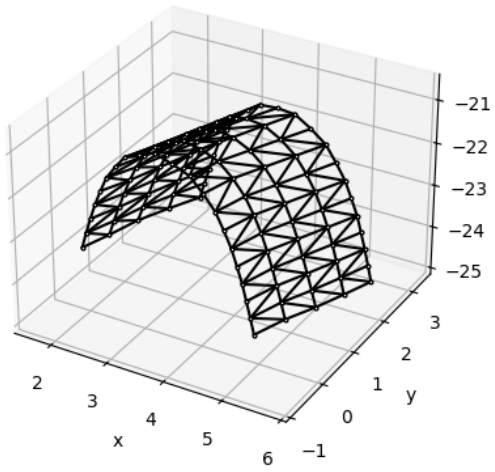

Fig. 18: Shell Simulation at t = 3.00 s, Load = 200N

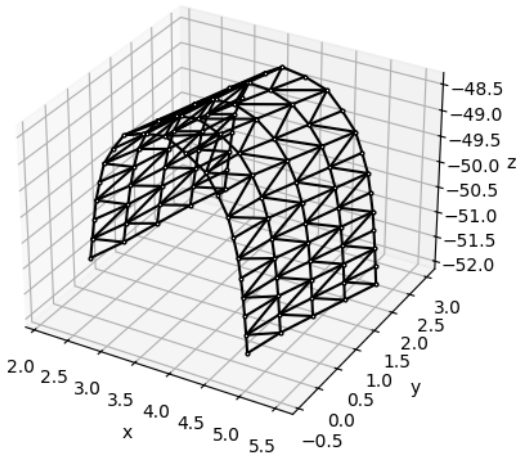

Fig. 19: Shell Simulation at t = 6.00 s, Load = 200N

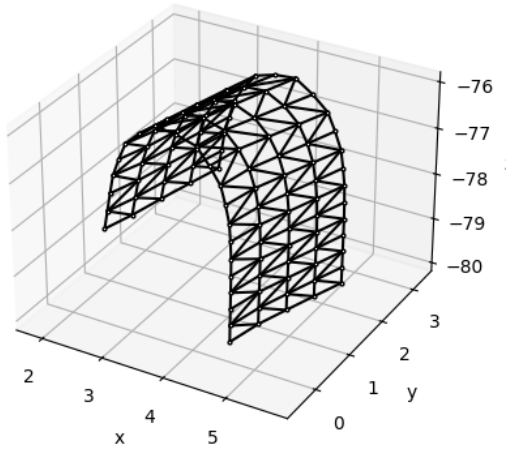

Fig. 20: Shell Simulation at t = 9.00 s, Load = 200N

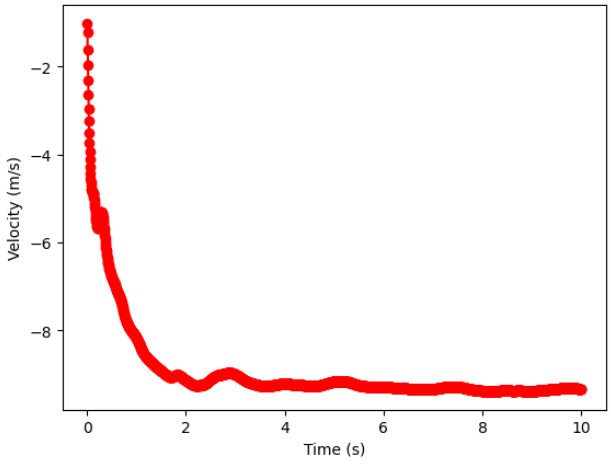

Fig. 21: Shell Simulation Terminal Velocity, Load = 200N

IV. DISCUSSION

An ideal parachute will provide enough drag for a low terminal velocity and have a compact geometry after deployment. The numerical solvers provided in the methodology section enable us to simulate the deployment of the parachute and find its steady state properties. This steady state is reached when the Z velocity becomes linear, meaning the parachute has reached terminal velocity for a given load and the shape of the canopy profile.

The results shown in figures 5 to 7 show the parachute shape in response to loads of 20, 200, and 2000 N being supported by the parachute. These are expected results as the parachute takes a more parabolic shape with higher pull downwards. Figures 8 to 10 to show the terminal velocity of parachutes and figures 11 to 13 show the relative extended height of the parachute. These two metrics show when the parachute final shape is reached, which is also when the terminal velocity is reached. The terminal velocity increased with load but the time to reach it decreased. Lighter load allow for more oscillation, while larger load dominates the simulation and the final state is reached much faster.

Load (N)	Terminal Velocity (m/s)	Time to Terminal Velocity (s)
20	-3.9	1.25
200	-3.9	0.75
2000	-10	0.4

TABLE I: Terminal velocity characteristics for different loads.

The performance of the parachute heavily relies on the fluid flow, material, and load. By using an approximation for the drag force coefficient, we restrict the focus of our initial study to the effects of the load for a given material using different numerical methods.

The shell simulations for 200N load has a much larger terminal velocity magnitude of around $9.4\frac{m}{s}$ is much larger than the terminal velocity predicted for the 200N load on a DER. Since the canopy shape of the shell during steady state has a significant potion oriented parallel to the relative fluid velocity, we expect it to have a lower drag than the DER simulation.

No of Load Sites	Terminal Velocity (m/s)
4	-9.4
6	-9.3

TABLE II: Terminal velocity for shell simulation with different loads configurations (200N)

Table II shows us that there is no significant changes when the load distribution is dispersed throughout the canopy or kept at the sides. Figures 14-16 and 18-20 provides the states of both simulations at different times. The canopy oscillates in shape by closing and opening. It also begins to rotate along the z-axis. This could be due to some asymmetry created from the generation of the discrete shell elements. This behavior could be mitigated by increasing the nuber of nodes and potentially using a better mesh layout.

V. POTENTIAL FORWARD WORK

Parachutes have a wide range of uses in various environments. To reflect the real complexities, the geometry, load, and fluid regime need to be more modeled much more accurately. This problem can also be solved with a classic CFD approach of Immersed Boundary Method but that is largely outside the scope of the methods learned in this class and more suited for a CFD course[4]. Alternatively, for supersonic flight, the Euler equations for compressible fluid flow can be used to model the fluid behavior and coupled with the structure behavior [7]. More accurate simulation work done on parachutes account for the porosity of the parachute [9]. This porous nature allows for some fluid to slip through the parachute canopy which enables a more stable descent.

Further work can also be done to study efficient control strategies for studying parachute behavior under a varying load condition [10]. It is possible to direct the movement of parachutes by pulling on lines at specific points. Previous work has been done to control the soft landing of a payload with controlled line pulls [8].

This problem is very dynamic and has fluids and structures coupling that rapidly changes the drag profile of the parachute. Advanced modeling analysis of parachutes like those covered in published works from NASA Ames are highly complex and require computational resources well beyond the scope of a graduate class but they do provide insight into expected behaviors possible within numerical analysis [2].

ACKNOWLEDGMENT

The core of the python code and the numerical logic used in this project is directly taken from the course materials provided by Professor M. Khalid Jawed for MAE 263F.

REFERENCES

[1] J. R. Cruz , "Estimates for the Aerodynamic Coefficients of Ringsail and Disk-Gap-Band Parachutes Operating on Mars ," Oct. 2017.
[2] J. Boustani, G. Anugrah, M. F. Barad, C. C. Kiris, and C. Brehm, "A Numerical Investigation of Parachute Deployment in Supersonic Flow," AIAA Science and Technology Forum and Exposition.
[3] L. Jiang et al., "Numerical Study on Aerodynamic Performance of Mars Parachute Models with Geometric Porosities," Space: science and technology, vol. 2022, Jan. 2022.

[4] Kim, Y., Peskin, C. S. (2006a). 2–D parachute simulation by the immersed boundary method. SIAM Journal on Scientific Computing, 28(6), 2294–2312. https://doi.org/10.1137/s1064827501389060

[5] G. Xing-long, Z. Qing-bin, T. Qian-gang, and Y. Tao, "Fluid-Structure Interaction Simulation of Parachute in Low Speed Airdrop," Proceedings of the World Congress on Engineering , vol. 3, no. WCE 2013, Jul. 2013.

[6] NASA Glenn Research Center. (n.d.). Velocity during recovery. https://www.grc.nasa.gov/www/k-12/VirtualAero/BottleRocket/airplane/rktvrecv.html

[7] Boustani, Jonathan, et al. "Fluid-structure interaction simulations of the ASPIRE SR01 supersonic parachute flight test." Aerospace Science and Technology 126 (2022): 107596.

[8] Stein, Keith R., et al. "Fluid-structure interactions of a round parachute: Modeling and simulation techniques." Journal of Aircraft 38.5 (2001): 800-808.

[9] Gao, Zheng, Richard D. Charles, and Xiaolin Li. "Numerical modeling of flow through porous fabric surface in parachute simulation." AIAA journal 55.2 (2017): 686-690.

[10] Dobrokhodov, Vladimir N., Oleg A. Yakimenko, and Christopher J. Junge. "Six-degree-of-freedom model of a controlled circular parachute." Journal of Aircraft 40.3 (2003): 482-493.